

Low viscosity, stable TiO₂ nano-fluid for oxidative photo-degradation of methylene blue

Ujjwal K Bhagat¹, Anuraj S. Kshirsagar¹, Ashish Gautam¹, Mehilal² and Pawan K Khanna^{1*}

¹Nano-chemistry Laboratory, Department of Applied Chemistry, Defence Institute of Advanced Technology (DIAT-DU), DRDO, Govt. of India, Pune 411025, India

²High Energy Materials Research Laboratory (HEMRL), Pune, India

*Corresponding author, E-mail: pawankhanna2002@yahoo.co.in

Received: 27 June 2016, Revised: 29 November 2016 and Accepted: 12 December 2016

DOI: 10.5185/amlett.2017.6960

www.vbripress.com/aml

Abstract

The present article highlights a simple and effective method for preparation of nano-fluid (NF) by employing long carbon chain fatty acid, PVP and ethylene glycol stabilized anatase phase TiO₂. The so-prepared nano-fluid (0.5 wt. %) was employed for advanced oxidative photo-degradation of MB with different concentrations (1-5 mL) under short (254 nm) and long UV (365 nm) irradiation against various concentrations (5, 15, 25 ppm). The maximum degradation efficiency observed was 88% and 71% under short and long UV irradiation respectively. The photocatalytic degradation of the MB was also studied by reaction kinetics. Initially, titania nanoparticles (NPs) were synthesized and characterized using various advanced tools such as UV-Visible, FTIR, Raman spectroscopy, BET, XRD, SEM/EDAX, TEM etc. for its size, surface area and morphological understanding. Copyright © 2017 VBRI Press.

Keywords: Anatase TiO₂ nanoparticles, TiO₂ nano-fluid, photo-catalysis, reaction kinetics, UV irradiation.

Introduction

Random increase in environmental pollution leads damage to the ecosystem and has become severe problem worldwide [1]. The harmful industrial effluents can cause severe health issues including cancer [2-5] and genetic mutation in living organism [5]. The industrial effluents are released in the water bodies which reduces the sunlight penetration and restricts the photosynthesis of aqueous plants [6]. There are various types of dyes (synthetic or artificial) which are a major and consistent part in the released industrial effluents, contaminating fresh water as well as causing serious harmful environmental hazards [7]. High demand of colored fabrics has led to extensive use of organic dyes in textile industries [8-10]. Methylene blue (MB) is one of the most widely used organic dye for the purpose of dyeing fabrics [7-10].

Post fabric treatment, the water is released from the industries into bigger reservoirs. Such dye contaminated water adversely affects the health of the living organisms. Eventually, the effluent comes in contact with the human beings and becomes cause of great concern for their health. The inhalation of such organic dye through drinking water may cause damage to the health including uneasiness in the respiratory tract [10], permanent injury as allergy [11], skin irritation [12], cell mutation leading to several other diseases such as leukemia [13]. The removal of such harmful dyes from the water is a big challenge and separation of water soluble dyes are required to be decomposed before joining main stream

water sources they therefore require proper chemical treatment for the safe degradation. The chemical treatment processes may be of varied nature however; advanced oxidation and reduction processes have attracted much attention [14-16]. Such oxidation and reduction processes involve formation of hydroxyl radical and super hydroxyl radical which reduce and oxidize a major part of organic dyes [17, 18]. There are several methods which can be utilized for treatment of such organic pollutants such as, Fenton process [19], ozonation [20, 21] and peroxone process [22] however, these methods are time consuming as well as expensive and therefore other method like degradation using photocatalytic materials such as TiO₂/ZnO more specifically metal oxides in the nano regime can be employed. Photo-catalysis helps to fasten the oxidizing and reducing process of the polluted water [23]. When UV irradiation and photo-catalysts used in combination, the *in-situ* generation of the hydroxyl radical helps to degrade such toxic organic pollutants [24, 25].

Titania nanoparticles are known to possess some peculiar properties like, self-cleaning [28], antibacterial coatings [29], hydrogen production [30], deodorization [31], hetero junction photo-voltaic cells for proper channeling of captured solar energy into electrical energy [32]. Apart from aforementioned properties, titania nanoparticles have ability to combat the issues related to water pollution *via* photocatalytic degradation [26, 27]. The most prominent feature of the titania is its band-gap which can absorb sunlight mostly good enough to affect the oxidation process due to its ability to generate

hydroxyl radicals under photonic energy. Decontamination of the polluted water from toxic organic dyes therefore has been heavily studied using titania and of late nano-particles of titania which has grabbed attention of the researchers worldwide [33, 34]. Titania is well known to exist in three crystalline phases *viz* anatase, rutile and brookite [35]. Among these three phases, anatase and rutile are mostly used and efficient materials when irradiated with the UV light [either short (254 nm) or long (365 nm)] whereas the catalytic activity possessed by amorphous titania is negligible [36-38]. The nano regime of anatase phase shows higher photocatalytic activity due to slowest recombination rate than nano rutile titania which has a slight higher recombination rate. The prolonged stay of the free electrons in the anatase titania make it a better photo-catalyst increasing its overall activity. On the other hand, rutile titania, due to deep trapping of the free electrons and longer stay of the holes reduces its overall activity [39, 40]. The smallest crystallite/ particle size and larger surface area of the titania nanoparticle is an important requirement for higher photocatalytic activity [41, 42]. The synthesized nanoparticles require high calcination up to 400°C for conversion of amorphous to crystalline anatase titania since photo-degradation ability of amorphous titania is negligible [36, 43, 44, 45].

NFs are well known for their modern applications as a coolant, friction reductant, antibacterial, nano-drug delivery, solar collectors etc. [46]. The nano-fluids can be called as 'next generation fluids' which are tailored for enhanced heat absorption activity [47]. Even though titania nanoparticles have been extensively exploited worldwide for their photocatalytic activity against the organic effluents [48], there are scarce reports on the utility of titania nano-fluid for photo-catalysis application [45(b, c)]. Chang *et al* [45b] have studied photocatalytic activity for degradation of methylene blue by using titania nano-fluid containing particle diameter of about 10 nm. The complete degradation of MB in less than 90 mins was effectively achieved. Similarly, Elsalamony *et al.* [45c] have described preparation of gamma-titania and its nano-fluids using two step method. Nano-fluid was employed for the photocatalytic MB degradation. Near about 90% photocatalytic degradation efficiency was observed in 240 mins when irradiated with UV.

As far as preparation of nano-fluids is concerned, they can be prepared either by single step, *in-situ* preparation using stabilizing agents or two-step with separate synthesis of nanoparticles and its conversion to nano-fluid using stabilizer [49]. The stabilizing agents are necessary to avoid or suppress the accumulation of the nanoparticles dispersed in the base fluid since nano particles have tendency to agglomerate, due to strong Van der Waals force between the particles [50, 51]. Stabilizers are well known to lower the surface tension of the base fluids responsible for their stability in a given liquid [51]. Oleic acid [52], Hexadecyltrimethyl ammonium bromide [53], Sodium dodecyl sulfate [54], Dodecyl trimethyl ammonium bromide [Dodecyl trimethyl ammonium bromide] [55] etc. are some of the important stabilizing agents widely used for slow sedimentation process with low or negligible agglomeration among the nanoparticles

dispersed in the base solvent [56]. The properties of the nanoparticles are said to be affected to some extent due to extensive use of the base solvent and stabilizers [57]. The flow of the nano-fluid is also an important entity to be studied which can be determined using the rheological behavior [58, 59]. The rheological studies can successfully predict the Newtonian and non-Newtonian behavior of nano-fluid [60-62]. The effect of temperature on the fluid flowability and the changes in the shear rate, stress and strain for the heat transfer applications have been studied by many researchers [63-66]. The rheology of the nano-fluid depends on the method of preparation, dispersion of the nanoparticles, base solvent and stabilizers employed [67-70].

In the present article, synthesis of anatase titania nanoparticles by sol-gel method and its conversion to the nano-fluid by employing stabilizers has been described. TiO₂ nano-fluid was applied for the oxidative photo-degradation of Methylene Blue, an organic dye. Titania NFs were employed in varied amounts to study their effect on the degradation of the Methylene Blue (MB) at different ppm (parts per million) levels. The comparative degradation study as well as complete degradation study along with the reaction kinetics of the MB under short and long UV irradiation is also presented. The rheological behavior of the nano-fluid has been included to understand the flow mechanism and its type. The use of titania nanofluid for the degradation of the organic dyes offer homogeneous dispersion in aqueous solution of an organic dye as compared to the use of undispersed nanoparticles as photocatalyst. Homogeneous dispersion of the nanoparticles because of easy solubility of the both solvents helps to provide more surface area for the redox reactions which eventually increases degradation efficiency. Other than this specific application of the nanofluid, it can be applied in variety of areas such as, in electronics, in mass transfer enhancement, coolants etc.

Experimental

Materials and characterization techniques

Titanium tetra-isopropoxide (TTIP), potato starch, absolute ethanol, iso-propanol, ethylene glycol, oleic acid, polyvinyl pyrrolidone (PVP) were all purchased from Sigma-Aldrich India Ltd. Mumbai and were used as received. The distilled water (18.2 MΩ) was used for synthesis, rinsing and cleaning purposes. Ultraviolet-visible spectrum was recorded on UV Specord 210 plus UV-visible spectrophotometer in 200-800 nm wavelength range for the analysis of nanoparticles and nano-fluids. Photoluminescence spectra of the nanoparticles was recorded on Agilent Technologies instrument in the range of 250-800 nm with 304 nm as an excitation wavelength. X-ray diffraction (XRD) analysis was carried out using Bruker A8 advanced instrument with specifications as Cu K α radiation ($\lambda = 0.1546$ nm) (@40 kV voltage and @120 mA current) at scanning rate of 2°/min between 2 θ range of 10-90°. Scanning electron microscope (SEM) analysis was carried out using Bruker Advanced (@300kV) model: JEOL/JSM-6360A. Transmission electron microscopy (TEM) measurement was carried out on Technai G2 Electron microscope (@200 kV). Fourier

transform infrared (FTIR) spectra was obtained using a Perkin Elmer Spectrum Two infrared spectrometer in range of $4000 - 400 \text{ cm}^{-1}$ for functional groups analysis. Raman spectra acquired using EZ Raman spectrometer in the range of $400 - 4000 \text{ cm}^{-1}$ for analysis of nanoparticles as well as nano-fluids. BET analysis was carried out using SSABETA-0405 BET Surface Area Analyzer under N_2 gas environment. The Nanophox (SympaTec) instrument used for the determination of nanoparticles distribution in DMF solution along with the stability of the nanoparticles dispersion in the nano-fluids for around 10 days. The density of the nano-fluid was measured using density meter Anton Paar-DMA 500, and the rheological studies were measured using Rheometer Physica MCR- 101 (plate diameter – 22 mm). Sono-chemical instrument (Sonics and Materials Inc. VCX 750, 20 KHz, 230VAC) was used for dispersion purpose of the nanoparticles within the base solvent in addition to stabilizers.

Synthesis of TiO_2 nanoparticles

The nano sized anatase TiO_2 particles were synthesized using a modified sol-gel method as reported by Khanna *et al* [71]. In present case, potato starch (0.5 g) pre-dissolved in 20 mL distilled water and TTIP (5 mL) was added dropwise into 2-propanol (30 mL). The whole reaction mixture was stirred for about 2 hours in an ice water bath maintained at $10\text{-}15^\circ\text{C}$. After two hours, the ice bath was removed and mixture was allowed to attain room temperature with continuous stirring. Meanwhile the formation of a milky white suspension (sol) was observed and in order to start the gelation process, the reaction mixture was allowed to stand for about 24-36 hours at room temperature. The as-formed gel was subjected to centrifugation at 5000 rpm to obtain white colored slurry. The slurry was washed thrice with methanol and twice with distilled water and then it was dried for 8-12 hours at $50\text{-}55^\circ\text{C}$ in an oven to obtain the fine white powder. Finally, in order to obtain phase pure and organic free titania nanoparticles white powder was sintered at 400°C .

TiO_2 Nano-fluid preparation

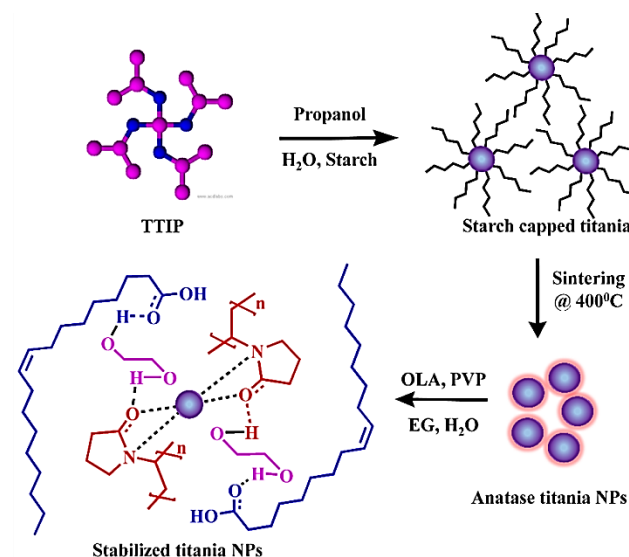
The nano-fluids (NFs) were prepared by a two-step method as reported by Khanna *et al* [72]. In 500 mL beaker, TiO_2 solution was prepared by dispersing TiO_2 NPs (2.0 g) in distill water (300 mL) and labeled as solution 'A'. In another beaker, PVP (0.5 g) was dissolved in distill water (100 mL) by sonication for 40 minutes and labeled as solution 'B'. Both the solutions were mixed together by sonication for another 20 minutes and resultant mixture (0.5 wt. %) was labeled as 'C'. In above mixture (solution C) was then added ethylene glycol (5 mL) and 4-6 drops of oleic acid as stabilizing agents and again sonicated for 5-10 min. The stable and well dispersed TiO_2 nano-fluid (NF) was then used for the further characterization and study. The stability of the nanoparticles was analyzed using particle size distribution method for about 10 days.

Results and discussion

The oxidation of titanium tetra-isopropoxide (TTIP) in presence of water and starch results in formation of starch

capped titania nanoparticles. The role of starch in the reaction is to control the growth of titania and provide oxygen rich surface [71]. The overcrowding of the starch molecules around titania facilitates suppression of particle growth and therefore, nano sized titania can be easily formed. Excess capping of the starch on titania could be disadvantageous in application point of view and hence sintering of the titania NPs is essential which helps to form phase pure and organic free titania NPs. In the present case, sintering of titania NPs at 400°C showed formation of anatase titania NPs. Phase pure titania NPs were converted to highly stable nano-fluid by using various stabilizing agents such as oleic acid (OLA), polyvinyl pyrrolidone (PVP) and ethylene glycol (EG).

Initial treatment of titania NPs with PVP possibly incorporate them randomly in the polymer network. Further addition of ethylene glycol could form hydrogen bonding with the oxygen atom of the carbonyl group in the PVP. Similarly, hydrogen bonding is also possible when OLA comes in contact with PVP and EG molecules and therefore, it is likely that titania nanoparticle gets surrounded by the molecules of PVP and long chain oleic acid bridged by ethylene glycol. This situation in presence of water helps titania nanoparticles to get much more stabilized due to high steric hindrance created by the organic molecules (surfactants) and hence titania NPs shows highly stable nano-fluid formation. The overall mechanism and possible interaction of titania NPs with the surfactants is depicted in **Scheme 1**.



Scheme 1. Synthesis of titania NPs and possible interaction of surfactant molecules with titania NPs.

Optical studies

The optical properties of the TiO_2 NPs were studied by UV-visible spectroscopy and photoluminescence spectroscopy. According to the literature reports the anatase titania nanoparticles are known to exhibit maximum absorbance around 390nm [73(a)]. In current study, the maximum absorbance observed for anatase TiO_2 NPs was near 304 nm resulting in a bandgap of 4.08eV (**Fig. 1A**). The blue shift obtained in UV-visible absorption values can be attributed to quantum

confinement effect due to the smaller particle size of the anatase titania. The UV-Visible spectroscopic study of as prepared nano-fluids also revealed presence of the well dispersed, stable and smaller TiO₂ NPs since they showed absorption near 306 nm. The light emitting properties was studied using Photoluminescence spectroscopy. The excitation at 304 nm for anatase titania was resulted in emission of about 376 nm (Fig. 1B) with a Stokes shift of about 72 nm indicating the absence of the Ti-OH states in the material.

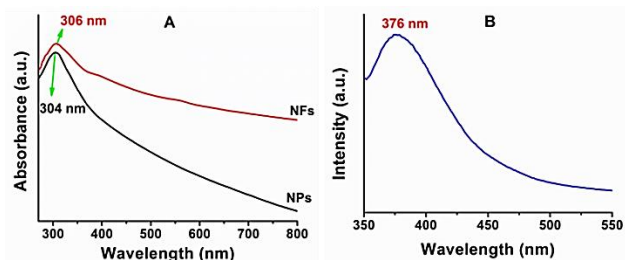


Fig. 1. UV-vis spectra of NPs and NF (A) and Photoluminescence spectrum of NPs (B).

However, NFs failed to show any useful emission properties mainly due to presence of large amount of organic capping from the base fluids composition. The bandgap of utilized TiO₂ NPs was calculated following equation 1 and the data is provided in Table 1 [73(b)].

$$E_g = \frac{hc}{\lambda} \quad (1)$$

where, E_g – bandgap, h – planck constant (6.626×10^{-34}), c – light velocity (3×10^8 m/s) and λ – maximum absorbance wavelength peak (nm).

Table 1. Optical properties of TiO₂ NPs and nano-fluid.

Optical Studies	Absorbance (nm) (NPs)	Bandgap (eV) from eq. 1	Absorbance (nm) (NF)	Bandgap (eV) from eq. 1
UV-Vis Spectroscopy	304	4.07	306	4.05
Photoluminescence	376	3.29	-	-

XRD analysis

The phase purity of the TiO₂ nanoparticles was confirmed from the XRD analysis. The XRD patterns of the so-obtained TiO₂ nanoparticles revealed formation of phase pure anatase titania nanoparticles (Fig. 2). The reflection peaks were indexed to (101), (004/112), (200), (105), (204) indicating formation of tetragonal crystal structure.

The sintering of the as-prepared nanoparticles leads to greater crystallinity without any adverse effects on the diffraction peaks. The crystallite size of the anatase titania NPs was calculated by using Scherrer formula (equation 2) [74];

$$D = \frac{0.9\lambda}{\beta \cos \theta} \quad (2)$$

where, D = crystallite size; λ = X-rays wavelength (Cu); β = FWHM; θ = diffraction angle.

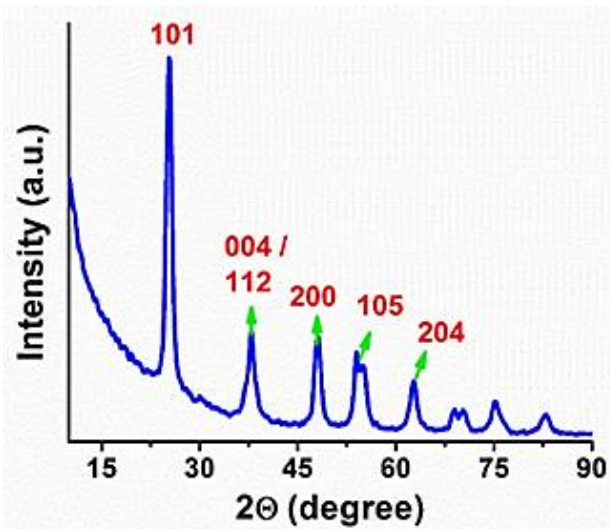


Fig. 2. XRD pattern of TiO₂ NPs sintered at 400°C.

The average particle size obtained by XRD data was found to be about 8.06 nm for the nanoparticles sintered at 400°C. The lattice parameters were calculated using the Bragg's equation (equation 3) and presented in Table 2 [75]

$$\lambda = 2d \sin \theta \quad (3)$$

where, λ = X-rays wavelength (Cu), d = inter planer distance, θ = diffraction angle. The lattice distance obtained for (101) diffraction plane was calculated to be 0.35 nm.

Table 2. XRD diffraction peaks and lattice parameter.

Diffraction Planes	2θ (degree)	Crystallite Size (nm)	Av. Crystallite Size (nm) [XRD]	d- Spacing (nm)	B cos θ (radians)	sin θ (degrees)	Particle Size (nm) [WH]
101	25.31	6.9	8.06	0.3514	0.0222	0.2189	8.54
004/112	37.92	12.4		0.2369	0.0123	0.3249	
200	47.95	7.4		0.1894	0.0208	0.4062	
105	54.07	6.3		0.1693	0.0244	0.4545	
204	62.59	7.3		0.1482	0.0210	0.5194	

The particle size and lattice strain of the titania NPs was also determined by employing UDM model of the Williamson-Hall (WH) analysis. The W-H plot (Fig. S1) of the titania NPs revealed the average particle size of about 8.54 nm. The W-H formula (equation 4) was used for the particle size calculation as well as lattice strain determination [76].

$$\beta \cos \theta = \left[\frac{k\lambda}{D} \right] + 4\epsilon \sin \theta \quad (4)$$

where, λ = X-rays wavelength (Cu), d = inter planer distance, θ = diffraction angle, D – crystallite size, β – FWHM, ϵ – lattice strain, $k = 0.9$.

Infrared spectroscopic studies

Titania nanoparticles was analyzed by FTIR in order to understand the presence of the functional groups on the surface of the NPs. The FTIR was recorded in the wavenumbers in the range of 400 cm⁻¹ to 4000 cm⁻¹

(Fig. S2). The major peaks observed near 2924-2850 cm^{-1} , 1635 cm^{-1} and 1040 cm^{-1} are ascribed to C-H symmetric and asymmetric stretching, C=O and C-O stretching frequencies respectively [71]. The bands at 1115 cm^{-1} and 900 cm^{-1} to 500 cm^{-1} was assigned to the asymmetric, symmetric stretching and the bending modes of Ti-O-Ti [76-79]. The absence of band near 3452 cm^{-1} and 1400 cm^{-1} indicated that the nanoparticles are free of the surface hydroxyl groups [77]. The presence of broad peak near 3380-3280 cm^{-1} was due to the hydroxyl groups of the potato starch. The functional groups along with their respective peaks are presented in Table S1.

Raman studies

As reported by Ohsaka *et al.*, phase pure anatase titania shows six Raman active modes (A1g + 2B1g + 3Eg) [80] with Raman peaks aligned at 144 cm^{-1} (Eg), 197 cm^{-1} (Eg), 399 cm^{-1} (B1g), 513 cm^{-1} (A1g), 519 cm^{-1} (B1g), and 639 cm^{-1} (Eg). The Raman spectrum of anatase phase TiO₂ NPs and NFs is shown in Fig S3. Five out of six Raman active modes were observed in the Raman spectrum with prominent peaks at 133, 187, 387, 506, 627 cm^{-1} . No other bands were observed in case of titania nanoparticles while in the spectrum of the NF, in addition to above, other bands were also observed due to presence of PVP, Oleic acid and Ethylene Glycol. The values of Raman active modes of the titania NPs and NF are given in Table S2 [81-83].

Electron microscopic studies

Surface morphology and stoichiometric ratios of titanium and oxygen of the titania nanoparticles were analyzed by scanning electron microscope (SEM) and EDX (Fig. 3). In SEM, the spherical nanoparticles with usual clustering were observed at scale bar of 30 nm. The particle size found to be about 8-13 nm and is well matched with the size calculated from XRD [8.06 nm], WH plot [11.59 nm], BET [10.68 nm] and Particle size analyzer [9 nm]. The EDX analysis indicate that the percentage oxygen is about three-fold higher than that of the titanium. The oxygen richness found in the sample was due to presence of the starch molecules over the surface of the titania NPs.

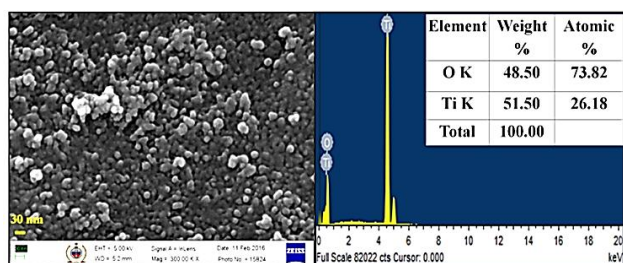


Fig. 3. SEM and EDX analysis of the titania nanoparticles.

The morphology of the titania nanoparticles was further studied by transmission electron microscopy (Fig. 4). TEM analysis also revealed spherical shape with the size of about 9-12 nm which was in good agreement with SEM [8-13 nm], XRD [8.06 nm], WH plot [11.59 nm], BET [10.68 nm] and particle size analyzer [9 nm]

results. The d-spacing about 0.3548 nm was calculated using the line profile plot and was in good agreement with the values estimated using Braggs equation for the (101) crystal plane.

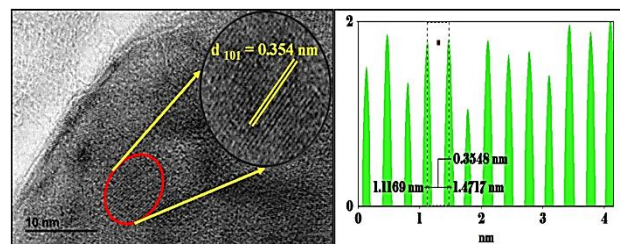


Fig. 4. TEM image and line profile plot of the titania nanoparticles.

BET analysis

Specific surface area (SSA) of the anatase TiO₂ nanoparticles was measured by BET analyzer. With reference to the result obtained (Table 3, Fig. S4), potato starch coated nanoparticles have surface area of 132.79 $\text{m}^2 \text{g}^{-1}$ with the particle size of 10.68 nm (calculated using BJH formula i.e. equation 5 [71] and Sauter's formula equation 6) [84]

$$T_{BET} = \frac{6000}{\rho \cdot SSA} \quad (5)$$

$$S_{XRD} = \frac{6000}{\rho \cdot D_{XRD}} \quad (6)$$

where D_{BET} – particle diameter in nm, SSA- the surface area of the nanoparticles in $\text{m}^2 \text{g}^{-1}$, and ρ is the theoretical density in g cm^{-3}) and D_{XRD} - crystallite size (calculated from Scherrer formula) and S_{XRD} - surface area of the nanoparticles in $\text{m}^2 \text{g}^{-1}$ calculated from XRD. The particle size calculated from BET analysis was also compared with the crystallite size calculated from XRD and it was observed to be larger. The difference in size can be assumed to be due to the agglomeration of the NPs. The degree of agglomeration among the nanoparticles can be calculated using the formula (equation 7 and 8) [85, 86a].

$$Interface\ area = \frac{S_{XRD} - S_{BET}}{2} \quad (7)$$

$$\frac{1}{F} = \frac{S_{BET}}{S_{XRD}} \quad (8)$$

where, interface area in $\text{m}^2 \text{g}^{-1}$ and S_{XRD} is the surface area calculated from crystallite size using the Scherrer equation 1, whereas S_{BET} is the specific surface area obtained from BET analysis and $1/F$ is the degree of agglomeration.

Table 3. Specific surface area, particle and crystallite size and interface area of the titania nanoparticles.

Sample	Size (nm)			SSA ($\text{m}^2 \text{g}^{-1}$)			Interface area ($\text{m}^2 \text{g}^{-1}$)	1/F
	XRD	WH plot	BET	XRD	WH plot	BET	($S_{XRD} - S_{BET}$)	S_{BET} / S_{XRD}
TiO ₂ NPs	8.06	8.55	10.68	164.93	165.89	132.79	32.55	0.8026

Particle size analyzer

The particle size distribution of the titania nanoparticles was determined using the particles size analyzer by dispersing NPs in DMF (Fig. S5). The average size distribution of the TiO₂ nano-particles was found in the

range of 2-20 nm and the maximum size distribution was observed to be at 6 nm. Such observations related well with findings of XRD and SEM analysis. **Fig. S5** shows the particle size distribution of the sample and relative peak width. The results so obtained also correlate with particle sizes calculated using XRD [8.06 nm], W-H plot [11.59 nm], SEM [8-13 nm], TEM [9-12 nm] and BET [10.68 nm] analysis.

Rheological study of TiO₂ nano-fluid

In order to understand the behavior of the titania nano-fluid, rheological parameter was measured. The nano-fluids were tested against varying parameters to study the occurrence of changes with respect to viscosity, shear rate, shear stress, torque and speed. So-prepared titania nano-fluid revealed Newtonian behavior as it was evident from all of the tests conducted at various temperatures (27, 35 and 43°C) presented in the **Fig. 5 (A-E)**. A plot of shear stress with shear rate (**Fig. 5A**) at various temperatures indicate the directly proportional relation between two entities as graph shows linear line. According to the **Fig. 5B** constant viscosity was observed with increasing torque and temperature. The increase in temperature resulted in increased value of torque. Similar observation was obtained when shear rate was plotted against viscosity.

Fig. 5C infers constant viscosity with increasing shear rate. Direct proportional relation was observed by plotting temperature against shear rate and with increased temperature shear rate found to be increased as shown in **Fig. 5D**. Increasing speed showed no effect on the viscosity values and it was found to be stable even speed was increased along with temperature (**Fig. 5E**). All these parameters emphasizing on typical Newtonian behavior of the nano-fluid.

Stability of nano-fluid

Stability of the nano-fluid is major concern which can decide the applicability of the nano-fluid in particular area and therefore, it was imperative to test as-prepared nano-fluid for stability. The stability of the titania nano-fluid

was investigated using the particle size analyzer over a period of ten days without disturbing the sample in the cuvette [**Fig. 6 (a)**]. The particle size distribution obtained for the period of the ten days clearly confirms the highly stable dispersion of the titania. although the initial TiO₂ size domain was of about 10-15 nm, they tend to agglomerated during their formulation to NFs. Thus the higher particle size distribution (35-40 nm) observed was due to the clustering of the nanoparticles in the sample. The nearly stable values of the particle size distribution over the period of ten days confirms high stability of the as-prepared nano-fluid. The formation of agglomerates can be assumed due to the presence of stabilizing agents i.e. PVP, ethylene glycol and oleic acid. The capping of the titania NPs by multiple organic molecules generally leads to the formation of dense coating over the particle surface. The dense coating of the surfactant over titania surface actually responsible for the generation of Brownian movement of the nanoparticles present in the sample. The sterically hindered nanoparticles can easily repel each other and therefore, a continuous movement of the particles was established which helps nanoparticles to remain dispersed all the time without flocculation [86b-86d]. The mechanism of the nano-fluid stabilization is depicted in the **Fig. 6(b)**.

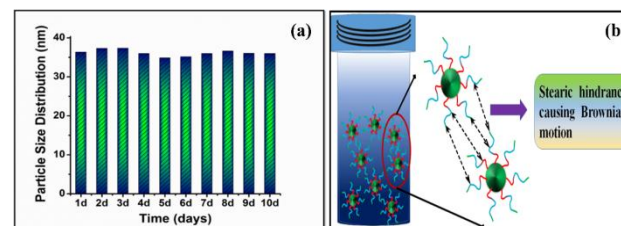


Fig. 6. (a) Stability of the nano-fluids over a period of ten days, (b) schematic showing stabilization process of titania NPs.

The density (**Fig. S6A**) and specific gravity (**Fig. S6B**) changes occurred with respect to temperature were also measured to understand the effect of oleic acid on the nano-fluid. The decrease in density and specific gravity occurred with increase in temperature. The effect of oleic

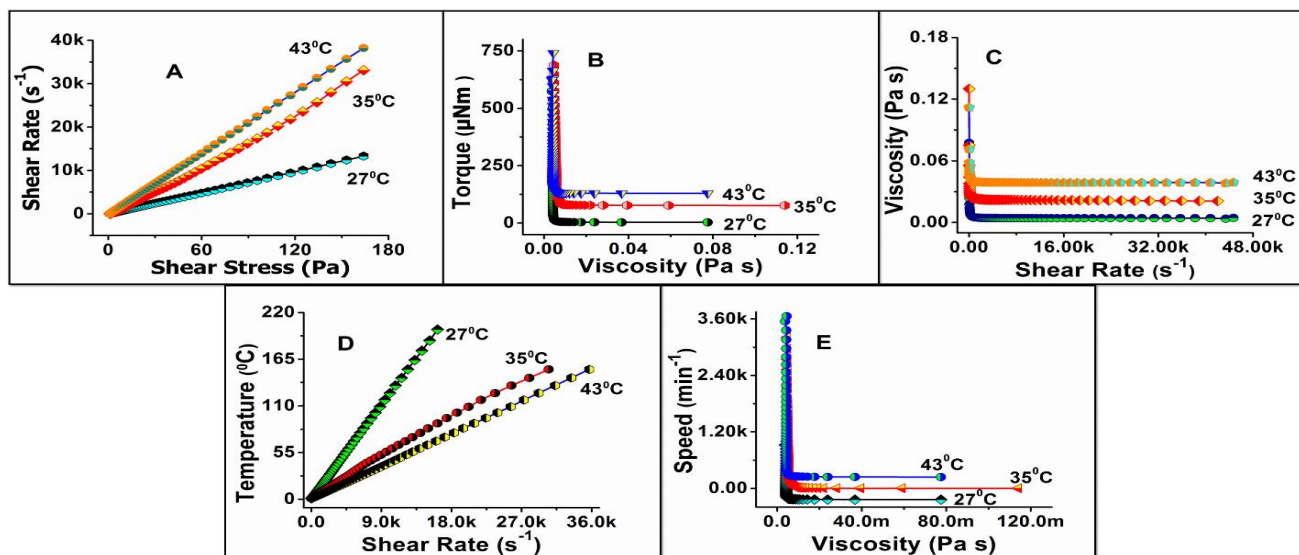


Fig. 5. Rheology study of the nano-fluid at various temperature.

acid observed to increase the density and specific gravity of the nano-fluid at all temperature but when temperature is increased, both the entities showed decrement in their respective values. The oleic acid helped in stabilizing the nanoparticles in the base solvent mixture.

Contact angle

The water contact angle measurement was done in order to understand the property of so prepared nano-fluids when in contact with glass surfaces. A single layer of the nano-fluid was cast on a glass slide and kept for drying off the excess liquid. The results indicate a low contact angle (32.57° i.e. hydrophilic) which infer good wetting and adhesiveness with high free surface energy, presented in **Fig. S7**.

Photocatalytic activity

The photocatalytic activity of titania nano-fluid was studied against Methylene Blue (**Fig. S8**) under short (254 nm) and long (365 nm) UV irradiation. It is well known that interaction of photons with TiO_2 available in the NF facilitates the excitation and transfer of electrons from valence band to conduction band [87]. The energy provided is often higher than its bandgap (3.2eV), which helps in generation of free electrons and holes over the catalyst surface along with hydroxyl radicals. Slow recombination rate of electron hole pair is the prime requirement to effectively degrade industrial effluent. During the catalytic degradation process, holes will capture electrons and oxidize pollutant molecules generating OH radicals. The excited electrons will degrade organic dyes (or the pollutant) either by the reduction process or might take part in reaction with the O_2 present on the catalyst surface to produce superoxide anion. The superoxide so generated will eventually degrade the effluent. The degradation process can be explained as shown below in equations 9-13 ($h\nu$ = photon energy; e^- = electrons and h^+ = holes) and in **Scheme 2**:



Vast literature is available for dye degradation using titania nanoparticles or its nano-fluid. The degradation of MB dye has also been studied by many researchers thereby making the current studies more straight forward. Table S3 presents some of the results from the literature. The percent efficiency (η) of the photo-degradation was calculated using following formula (equation 14): [71]

$$\left(\frac{A_0 - A_t}{A_0}\right) \times 100 = \eta (\text{efficiency}) \quad (14)$$

where, A_0 = absorbance intensity of dye solution before the UV treatment, A_t = absorbance of dye solution after UV treatment at time t. The energy of activation was calculated using Arrhenius equation (equation 15) [71]

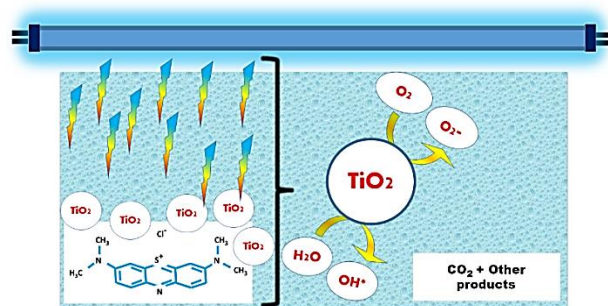
$$\log k = -\left(\frac{E_a}{2.303 \cdot R \cdot T}\right) \quad (15)$$

where, k = reaction rate constant (min^{-1}), E_a = reaction energy of activation (kJ mol^{-1}), R = gas constant and T = reaction temperature (kelvin). The reaction kinetics of the catalytic degradation of the industrial effluent calculated using the first order rate kinetics (equation 16 and 17). [71]

$$C = C_0 e^{-kt} \quad (16)$$

$$-\ln\left(\frac{C}{C_0}\right) = kt \quad (17)$$

where, C_0 = initial dye concentration (ppm), C = dye concentration at time t (min), k = reaction rate constant (min^{-1}), t = time (min).



Scheme 2. Methylene Blue degradation by anatase titania nano-fluid.

Activity under short UV irradiation

The characterization studies of the as-prepared nanofluid have revealed the presence of titania nanoparticles of particle size 10-15 nm exhibiting absorbance peak at about 306 nm (band gap = 4.05 eV). This clearly reveals that for photodegradation study the irradiation light below 300 nm will be much beneficial. This may help to easy excitation and transfer of the electrons which are further utilized for degradation process. In view of the above, here in present case short UV irradiation (wavelength 254 nm) was employed for the degradation process. The photocatalytic activity of the titania nano-fluid under short UV irradiation was evaluated against MB (methylene blue). The dual absorbance peak in methylene blue at 664 and 615 nm is due to conjugated hetero-poly aromatic linkage system of sulphur and nitrogen and has been attributed to transition from n to p^* (lone pair electrons of nitrogen atom) and p to p^* (conjugated double bonds system of aromatic rings). The absorption peak at 664 nm was monitored by UV-Visible spectroscopy for study of degradation using titania nano-fluid as catalyst. The UV irradiation (short wavelength 254 nm) caused decrease in the absorbance intensity indicating the degradation of the dye. Initially photocatalytic activity of 1.0 mL of nano-fluid was measured against 05, 15 and 25 ppm of dye solution (**Fig. 7 A, B, C**) for 270 min with interval of 30 min. According to the degradation results it was found that, the highest degradation efficiency was about 75.97 % for 15 ppm dye solution (**Fig. 7 B**) while degradation efficiency for 05 and 25 ppm was found to be about 61.43% and 47.84% respectively. The degradation efficiency for 5 and 25 ppm was found lower than that for 15 ppm dye solution and therefore, it was imperative to study the concentration

effect of nano-fluid catalyst on degradation efficiency of 15 ppm MB.

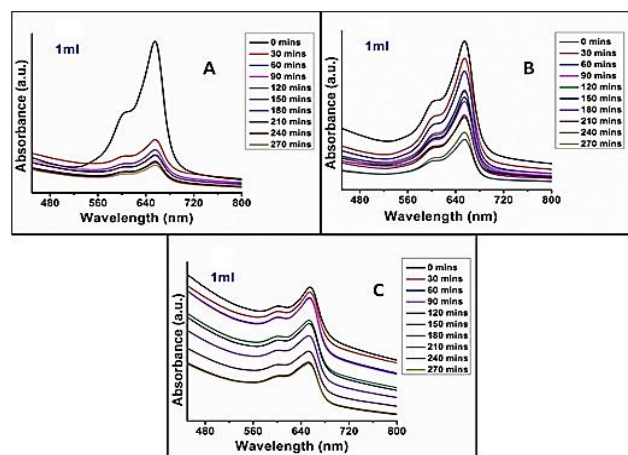


Fig. 7. Monitoring of degradation of (A) 5, (B) 15 and (C) 25 ppm MB solution using 1 mL of titania nano-fluid as photo-catalyst under short UV irradiation.

In order to study catalyst concentration effect, series of experiments were carried out using different concentrations of nano-fluid e.g. 1.5 to 5.0 mL nano-fluid against a fix concentration of MB solution (15 ppm). Results revealed (**Fig. 8 A-F**) that, the increase in the catalyst concentration increases the degradation efficiency of the MB degradation process (**Table S4**).

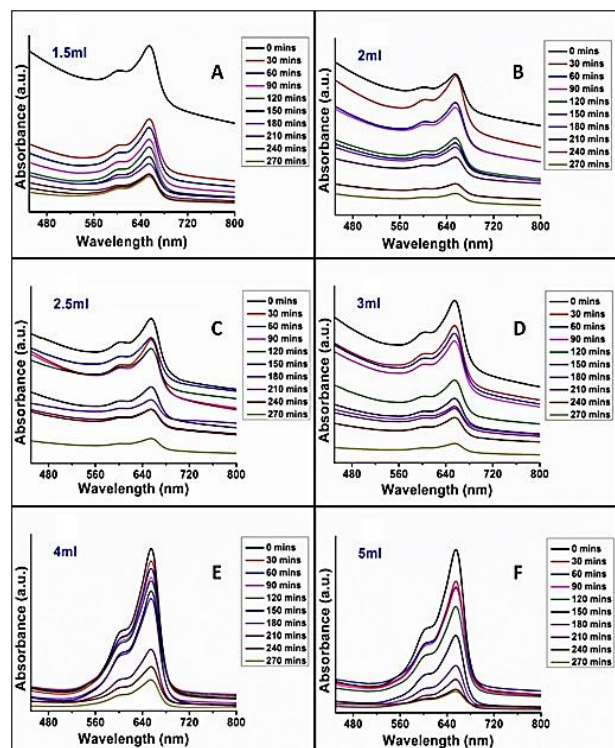


Fig. 8. Monitoring of degradation of 15 ppm MB solution using various concentrations of titania nano-fluid as photo-catalyst under short UV irradiation.

The highest efficiency obtained was 88 % with rate constant of 0.0179 min^{-1} and energy of activation of about $10026.99 \text{ kJmol}^{-1}$ for 3 mL of catalyst (**Fig. 8D**). Further addition of catalyst (4 and 5 mL) showed slight decrease

in the efficiency and therefore, it can be considered that 3 mL nano-fluid is optimum quantity to achieve maximum degradation of MB under short UV irradiation. Beyond 3 mL of nano-fluid, supersaturation of the catalyst hinders the reduction process during the degradation leading to decrease in the degradation efficiency. Almost in all cases, decrease in absorbance intensity with respect to time was observed indicating the effectiveness of nano-fluid as photo-catalyst irrespective of its concentration. The reaction kinetics of the degradation of MB under short UV irradiation was studied along with activation energy as well as C/C_0 vs time plots (**Fig. 9** and **10**). The decrease in rate constant and C/C_0 values with respect to time clearly confirms the degradation of MB under short UV irradiation.

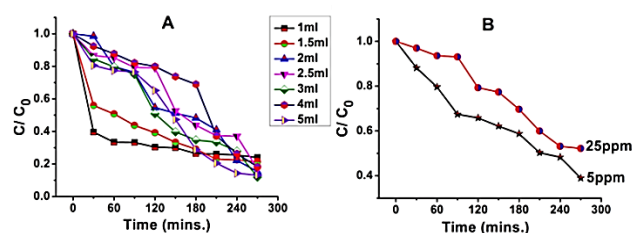


Fig. 9. C/C_0 vs time plots for (A) 15 ppm, (B) 5 ppm and 25 ppm MB degradation under short UV.

The photocatalytic degradation of the MB in presence of titania nanofluid and under short UV irradiation observed to give good results. This might be because of homogeneous dispersion of the nanofluid in aqueous solution of MB providing more surface area for the adsorption and desorption during the redox process. The values of rate constant and activation energy are presented in Table S4. The rate of the degradation process found to be nearly constant when nanofluid concentration was varied from 1-5 mL for 15 ppm MB solution except for 3 mL nanofluid where rate was observed to be lower with comparatively high activation energy.

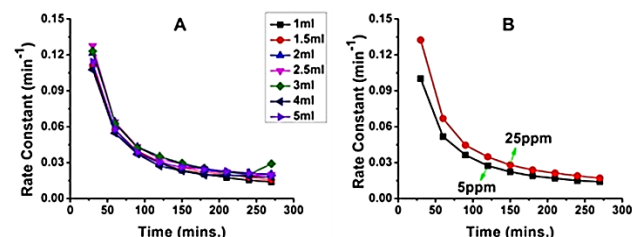


Fig. 10. Rate constant of (A) 15 ppm, (B) 5 ppm and 25 ppm MB degradation under short UV.

Activity under long UV irradiation

The photocatalytic degradation MB under the irradiation of short UV, nano-fluid revealed the highest degradation efficiency of 88% for 3.0 mL NF process. However, when the same process was carried out under UV irradiation with 365 nm wavelength (long UV) results were found to be much inferior. Three different sets of MB solutions (05, 15 and 25 ppm) were examined initially for 1 mL of nano-fluid catalyst for 270 min with interval of 30 min. (**Fig. 11 A, B** and **C**). Careful monitoring of degradation

process by UV-visible spectroscopy revealed only 65.75 % degradation efficiency for 5 ppm MB solution. On the other side 15 and 25 ppm MB solution showed rather unattractive 37.18 and 48.05 % degradation efficiency respectively. It was observed that at lower energy irradiation, 5 ppm MB solution showed maximum degradation efficiency. Therefore, 5 ppm MB solution was chosen to study effect of nano-fluid concentration on degradation process. A series of experiments by changing amount of nano-fluid were thus carried out (Fig. 12 A-F).

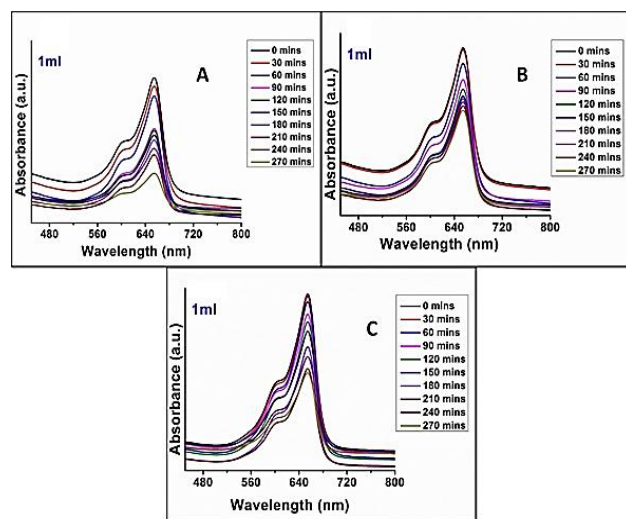


Fig. 11. Monitoring of degradation of (A) 5, (B) 15 and (C) 25 ppm MB solution using 1 mL of titania nano-fluid as photo-catalyst under long UV irradiation.

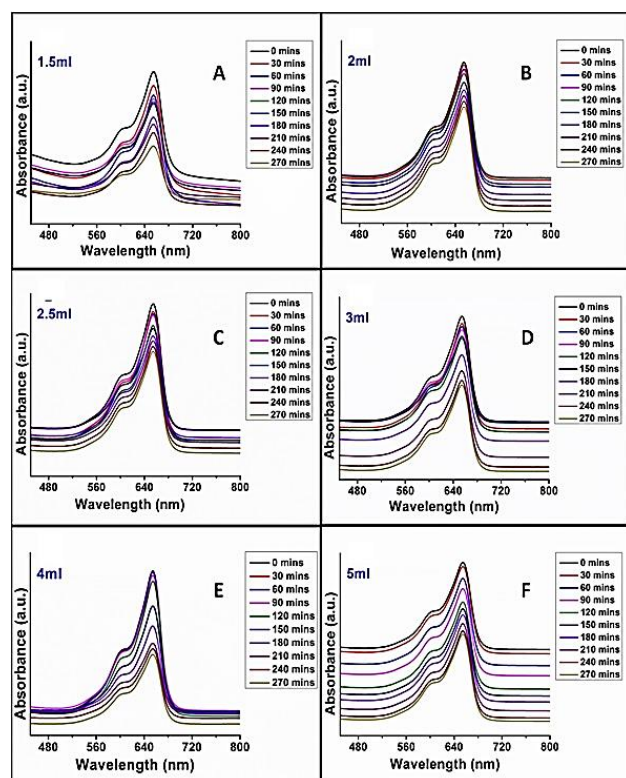


Fig. 12. Monitoring of degradation of 5 ppm MB solution using various concentrations of titania nano-fluid as photo-catalyst under long UV irradiation.

The increase in degradation efficiency was observed as concentration of nano-fluid was increased. The highest efficiency obtained was 71 % with rate constant of 0.0135 min^{-1} and energy of activation of about $10739.63 \text{ kJmol}^{-1}$ for 4 mL of catalyst under long UV irradiation. Furthermore, the reaction kinetics, activation energy, and C/C_0 vs time plots were also studied. The C/C_0 and rate constant vs time plots are presented in Fig. 13 and Fig. 14 respectively. These plots are clearly confirming the degradation of MB under long UV irradiation. The values of rate constant and activation energy are given in table S5.

The rate constant values obtained at various concentrations for degradation process using short and long UV irradiation are presented in figure 15 the highest rate constant was found by using 2.5 mL and 1 mL nano-fluid under short (Fig. 15 A) and long UV (Fig. 15 B) respectively.

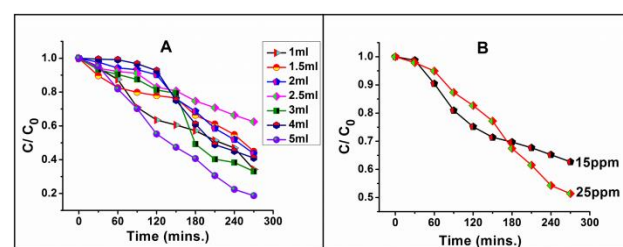


Fig. 13. C/C_0 vs time plots for (A) 15 ppm, (B) 5 ppm and 25 ppm MB degradation under long UV.

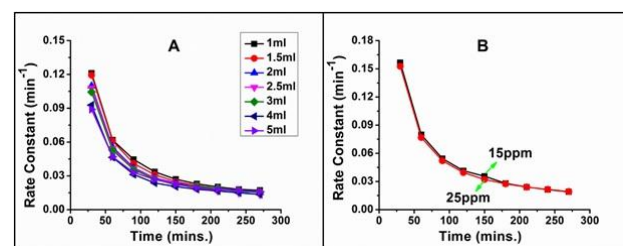


Fig. 14. Rate Constant of (A) 15ppm, (B) 5ppm and 25ppm MB degradation under long UV.

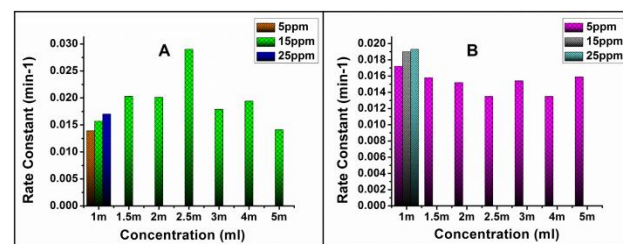


Fig. 15. Rate constant vs concentration of NF and MB (ppm) under short (A) and long UV (B).

The overall efficiency of the MB degradation is illustrated in Fig. 16 A for short UV irradiation and Fig. 16 B for long UV irradiation. Under short UV irradiation highest efficiency was obtained for 15 ppm MB solution using 3.0 mL nano-fluid catalyst whereas under long UV irradiation highest efficiency was achieved for 5 ppm dye solution while 4.0 mL nano-fluid was employed.

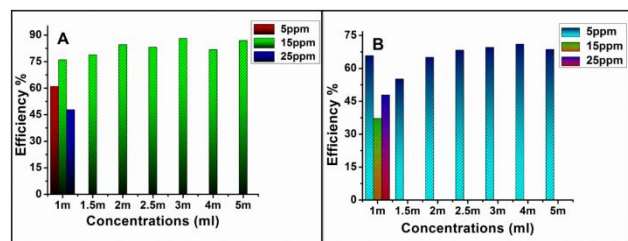


Fig. 16. Efficiency vs concentration of NF and MB (ppm) under short UV (A) and long UV (B).

Conclusion

Adopting a simple and modified sol-gel method, titania NPs were synthesized using potato starch as surfactant. Phase pure titania NPs obtained by sintering at 400°C, were converted to the highly stable nano-fluids. Oleic acid, PVP and ethylene glycol stabilized titania nano-fluids were successfully employed for degradation of MB under short and long UV. Varied concentrations of the MB solutions (5, 15 and 25 ppm) were examined for degradation under short and long UV irradiation in presence of various concentrations of the nano-fluid as photo-catalyst. Nano-fluid catalyzed degradation of MB showed higher degradation efficiency of about 88% and minimum of 76% under short UV irradiation (0.5 wt. % TiO₂ NF) however; slight lower degradation efficiency of 71% was observed under long UV irradiation. The rate of reaction was found to be about 0.0290 min⁻¹ under short UV while 0.0193min⁻¹ for long UV irradiation. Titania nano-fluid was successfully employed for degradation of MB under short and long UV however, there is wide scope to explore abatement of such pollutants by employing efficient and ecofriendly titania based photo-catalysts for waste water treatment.

Acknowledgements

The authors are grateful to the Vice Chancellor, DIAT for providing facility for the fulfillment of this research.

References

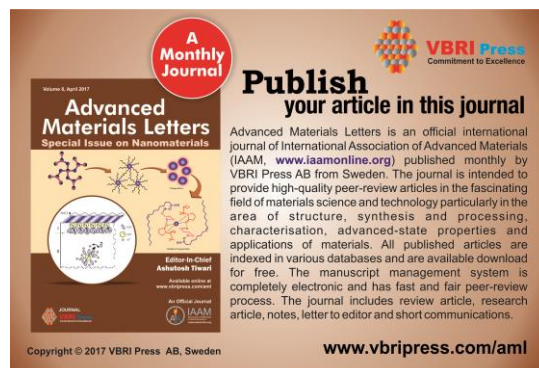
- Lefebvre, O.; Moletta, R.; *Water Research*, **2006**, *40*, 3671. DOI: [10.1016/j.watres.2006.08.027](https://doi.org/10.1016/j.watres.2006.08.027)
- Estlander, T.; *Contact Dermatitis*, **1998**, *18*, 290. DOI: [10.1111/j.1600-0536.1988.tb02836.x](https://doi.org/10.1111/j.1600-0536.1988.tb02836.x)
- Ghaly, A.E.; Ananthashankar, R.; Alhattab, M.; Ramakrishnan, V.V.; *J Chem.Eng. Process Technol*, **2014**, *5*, 1. DOI: [10.4172/2157-7048.1000182](https://doi.org/10.4172/2157-7048.1000182)
- Gray, M.; Black, J.M.; Baharestani, M.M.; Bliss, D Z.; Colwell, J C.; Goldberg, M; Evans K.L.K; Logan, S.; Ratliff, C.R.; *J Wound Ostomy Continence Nurs.*, **2011**, *38*, 233. DOI: [10.1097/WON.0b013e318215f798](https://doi.org/10.1097/WON.0b013e318215f798)
- Ames, B.N.; *Science*, **1979**, *204*, 587. DOI: [10.1126/science.373122](https://doi.org/10.1126/science.373122)
- Kumar, K. V.; Ramamurthi, V.; Sivanesan, S.; *Dyes and Pigments*, **2006**, *69*, 102. DOI: [10.1016/j.dyepig.2005.02.005](https://doi.org/10.1016/j.dyepig.2005.02.005)
- Taddese, G.; *Environmental Management*, **2001**, *27*, 815. DOI: [10.1007/s002670010190](https://doi.org/10.1007/s002670010190)
- Hutzinger, The *Handbook of Environmental Chemistry* Volume 3 Part A; Springer-Verlag Berlin Heidelberg GmbH, **1980**. DOI: [10.1007/978-3-540-38522-6](https://doi.org/10.1007/978-3-540-38522-6)
- Houas, A.; Lachheb, H.; Ksibi, M.; Elaloui, E.; Guillard, C.; Herrmann, J.M.; *Applied Catalysis B: Environmental*, **2001**, *145*. DOI: [10.1016/S0926-3373\(00\)00276-9](https://doi.org/10.1016/S0926-3373(00)00276-9)
- Evgenov, OV; Sager, G; Bjertnaes, L.J.; *CritCare Med.*, **2001**, *29*, 374.

DOI: [10.1097/00003246-200102000-00028](https://doi.org/10.1097/00003246-200102000-00028)

- Abramson, H.A; Gorix, M. H.; *J. Phys. Chem.*, **1940**, *44*, 1094. DOI: [10.1021/j150405a008](https://doi.org/10.1021/j150405a008)
- Stradling, B.; Aranha, G.; Gabram, S.; *The American Journal of Surgery*, **2002**, *184*, 350. DOI: [10.1016/S0002-9610\(02\)00945-5](https://doi.org/10.1016/S0002-9610(02)00945-5)
- Shaw, M. W.; *Annual Review of Medicine*, **1970**, *21*, 409. DOI: [10.1146/annurev.me.21.020170.002205](https://doi.org/10.1146/annurev.me.21.020170.002205)
- Rafatullah, M.; Sulaiman, O., Hashim R., Ahmad, A; *Journal of Hazardous Materials*, **2010**, *177*, 70. DOI: [10.1016/j.jhazmat.2009.12.047](https://doi.org/10.1016/j.jhazmat.2009.12.047)
- Gupta, V.K.; Suhas; *Journal of Environmental Management*, **2009**, *90*, 2313. DOI: [10.1016/j.jenvman.2008.11.017](https://doi.org/10.1016/j.jenvman.2008.11.017)
- Dutta, K.; Mukhopadhyay, S.; Bhattacharjee, S.; Chaudhuri, B.; *Journal of Hazardous Materials B*, **2001**, *84*, 57. DOI: [10.1016/S0304-3894\(01\)00202-3](https://doi.org/10.1016/S0304-3894(01)00202-3)
- Carp, O.; Huisman, C.L.; Reller, A.; *Progress in Solid State Chemistry*, **2004**, *32*, 33. DOI: [10.1016/j.progsolidstchem.2004.08.001](https://doi.org/10.1016/j.progsolidstchem.2004.08.001)
- Taleblian, N.; Nilforoushan, M.R.; *Thin Solid Films*, **2010**, *518*, 2210. DOI: [10.1016/j.tsf.2009.07.135](https://doi.org/10.1016/j.tsf.2009.07.135)
- Sun, J.H.; Sun, S.P.; Wang, G.L.; Qiao, L.P.; *Dyes and Pigments*, **2007**, *74*, 647. DOI: [10.1016/j.dyepig.2006.04.006](https://doi.org/10.1016/j.dyepig.2006.04.006)
- Robinson, T.; McMullan, G.; Marchant, R.; Nigam, P.; *Bioresource Technology*, **2001**, *77*, 247. DOI: [10.1016/S0960-8524\(00\)00080-8](https://doi.org/10.1016/S0960-8524(00)00080-8)
- Sarasa, J.;Roche, M. P.; Ormad, M. P.; Gimeno, E.; Puig, A.; Ovelheiro, J. L.; *Wat. Res.*, **1998**, *32*, 2721. DOI: [10.1016/S0043-1354\(98\)00030-X](https://doi.org/10.1016/S0043-1354(98)00030-X)
- Malik, P.K.; Saha, S.K.; *Separation and Purification Technology*, **2003**, *31*, 241. DOI: [10.1016/S1383-5866\(02\)00200-9](https://doi.org/10.1016/S1383-5866(02)00200-9)
- Li, Y.; Xie, W.;Hu, X.; Shen, G.; Zhou, X.; Xiang, Y.; Zhao, X.; Fang, P.; *Langmuir*, **2010**, *26*, 591. DOI: [10.1021/la902117c](https://doi.org/10.1021/la902117c)
- Konstantinou, I. K.; Albanis, T. A.; *Applied Catalysis B: Environmental*, **2004**, *49*, 1. DOI: [10.1016/j.apcatb.2003.11.010](https://doi.org/10.1016/j.apcatb.2003.11.010)
- Lachheb, H.; Puzenat, E.; Houas, A.; Ksibi, M.; Elaloui, E.; Guillard, C; Herrmann, J.M.; *Applied Catalysis B: Environmental*, **2002**, *39*, 75. DOI: [10.1016/S0926-3373\(02\)00078-4](https://doi.org/10.1016/S0926-3373(02)00078-4)
- Cermenati, L.; Pichat, P.; Guillard, C.; Albini, A.; *J. Phys. Chem. B*, **1997**, *101*, 2650. DOI: [10.1021/jp962700p](https://doi.org/10.1021/jp962700p)
- Rome'as, V.; Pichat, P.; Guillard, C.; Chopin, T.;Lehaut, C.; *Ind. Eng. Chem. Res.*,**1999**, *38*, 3878. DOI: [10.1021/ie990326k](https://doi.org/10.1021/ie990326k)
- Ohko, Y.; Saitoh, S.; Tatsuma, T.; Fujishima, A.; *Journal of The Electrochemical Society*, **2001**, *148*, B24. DOI: [10.1149/1.1339030](https://doi.org/10.1149/1.1339030)
- Fu, G.; Vary, S.P.; Lin C.T.; *J. Phys. Chem. B*, **2005**, *109*, 8889. DOI: [10.1021/jp0502196](https://doi.org/10.1021/jp0502196)
- Gupta, S. M.; Tripathi M.; *Chinese Science Bulletin*, **2011**, *56*, 1639. DOI: [10.1007/s11434-011-4476-1](https://doi.org/10.1007/s11434-011-4476-1)
- Pichat, P.; Disdier, J.; Hoang-Van, C.; Mas, D.; Goutailler, G.; Gaysse C.; *Catalysis Today*, **2000**, *63*, 363. DOI: [10.1016/S0920-5861\(00\)00480-6](https://doi.org/10.1016/S0920-5861(00)00480-6)
- Kim, Y.G.; Walker, J.; Samuelson, L.A.; Jayant Kumar, J.; *Nano Letters*, **2003**, *3*, 523. DOI: [10.1021/nl0259535](https://doi.org/10.1021/nl0259535)
- Watanabe, T.; Fukayama, S.; Miyauchi, M.; Fujishima, A.; Hashimoto, K.; *Journal of Sol-Gel Science and Technology*, **2000**, *19*, 71. DOI: [10.1023/A:1008762121743](https://doi.org/10.1023/A:1008762121743)
- Getoff N.; *Proc. Indian Acad. Sci. (Chem. Sci.)*,**1993**, *105*, 373. DOI: [10.1007/BF03040811](https://doi.org/10.1007/BF03040811)
- Liu, L.; Zhao, H.; Andino, J.; Li, Y.; *ACS Catal.*,**2012**, *2*, 1817. DOI: [10.1021/cs300273q](https://doi.org/10.1021/cs300273q)
- Ambrus, Z.; Mogyoro'si, K.; Szalai, A.; Alapi, T.; Demeter, K.; Dombi, A.; Sipos, P.; *Applied Catalysis A: General*,**2008**, *340*, 153. DOI: [10.1016/j.apcata.2008.02.010](https://doi.org/10.1016/j.apcata.2008.02.010)

37. Reyes-Coronado, D.; Rodríguez-Gattorno, G.; Espinosa-Pesqueira, M.E.; Cab, C.; Coss, R. de.; Oskam, G.; *Nanotechnology*, **2008**, *19*, 145605.
DOI: [10.1088/0957-4484/19/14/145605](https://doi.org/10.1088/0957-4484/19/14/145605)
38. Zhang, Q.; Gao, L.; Guo, J.; *Applied Catalysis B: Environmental*, **2000**, *26*, 207.
DOI: [10.1016/S0926-3373\(00\)00122-3](https://doi.org/10.1016/S0926-3373(00)00122-3)
39. Akira Yamakata, A.; Vequizo, J.J.M.; Matsunaga, H.; *J. Phys. Chem. C*, **2015**, *119*, 24538.
DOI: [10.1021/acs.jpcc.5b09236](https://doi.org/10.1021/acs.jpcc.5b09236)
40. Zhang, J.; Zhou, P.; Liu, J.; Yu, J.; *Phys.Chem.Chem.Phys.*, **2014**, *16*, 20382.
DOI: [10.1039/c4cp02201g](https://doi.org/10.1039/c4cp02201g)
41. Sun, J.; Gao, L.; Zhang, Q.; *J. Am. Ceram. Soc.*, **2003**, *86*, 1677.
DOI: [10.1111/j.1151-2916.2003.tb03539.x](https://doi.org/10.1111/j.1151-2916.2003.tb03539.x)
42. Ashutosh Tiwari, Y.K. Mishra, H. Kobayashi, A.P.F. Turner (Eds), In the Intelligent Nanomaterials, 2nd Edition, John Wiley & Sons, USA, **2016**.
43. Su, C.; Hong, B.Y.; Tseng, C.M.; *Catalysis Today*, **2004**, *96*, 119.
DOI: [10.1016/j.cattod.2004.06.132](https://doi.org/10.1016/j.cattod.2004.06.132)
44. Wang, C.C.; Ying, J.Y.; *Chem. Mater.*, **1999**, *11*, 3113.
DOI: [10.1021/cm990180f](https://doi.org/10.1021/cm990180f)
45. (a) Zhu, Y.; Zhang, L.; Gao, C.; Cao, L.; *Journal of Materials Science*, **2000**, *35*, 4049.
DOI: [10.1023/A:1004882120249](https://doi.org/10.1023/A:1004882120249)
(b) Chang, H.; Su, C.; Lo, C-H.; Chen, L-C.; Tsung; T-T.; Jwo, C-S. *Materials Transactions*, **2004**, *45*, 12, 3334-3337.
DOI: [10.2320/matertrans.45.3334](https://doi.org/10.2320/matertrans.45.3334)
(c) Elsalamony, R. A.; Morsi, R. E.; Alsabagh, A.M. *Journal of Nanofluids*, **2015**, *4*, 1-7,
DOI: [10.1166/jon.2015.1179](https://doi.org/10.1166/jon.2015.1179)
46. (a) Taylor, R.; Coulombe, S.; Otanicar, T.; Phelan, P.; Gunawan, A.; Lv, W.; Rosengarten, G.; Prasher, R.; Tyagi, H. *Journal of Applied Physics*, **2013**, *113*, 011301.
DOI: [10.1063/1.4754271](https://doi.org/10.1063/1.4754271)
(b) Zhou, J.; Wu, Z.; Zhang, Z.; Liu, W.; Xue, Q.; *Tribol. Lett.* **2000**, *8*, 213.
DOI: [10.1155/2014/785680](https://doi.org/10.1155/2014/785680)
(c) Jones, N.; Ray, B.; Ranjit, K.T.; Manna, A.C.; *FEMS Microbiol. Lett.* **2008**, *279*, 71.
DOI: [10.1111/j.1574-6968.2007.01012.x](https://doi.org/10.1111/j.1574-6968.2007.01012.x)
(d) Liu, Y.; Zhou, Y.; Tong, M.; ZhouX., *Microfluid. Nanofluid.* **2009**, *7*, 579.
DOI: [10.1007/s10404-009-0423-8](https://doi.org/10.1007/s10404-009-0423-8)
47. Jang, S.P.; Choi, S.U.S.; *Applied Thermal Engineering*, **2006**, *26*, 2457.
DOI: [10.1016/j.applthermaleng.2006.02.036](https://doi.org/10.1016/j.applthermaleng.2006.02.036)
48. Liu, S.; Yu, J.; Jaroniec, M.; *Chem. Mater.*, **2011**, *23*, 4085.
DOI: [10.1021/cm200597m](https://doi.org/10.1021/cm200597m)
49. Songjun Li, Yi Ge, Ashutosh Tiwari, Shunsheng Cao (Eds), In the A Temperature-Responsive Nanoreactor, WILEY-VCH Verlag, USA, **2010**.
50. Wen, D.; Lin, G.; Vafaei, S.; Zhang, K.; *Particuology*, **2009**, *141*.
DOI: [10.1016/j.partic.2009.01.007](https://doi.org/10.1016/j.partic.2009.01.007)
51. Buongiorno, J.; Venerus, D.C.; Prabhat, N.; McKrell, T.; Townsend, J.; Christianson, R.; Tolmachev, Y.V.; Keblinski, P.; Hu, L.W.; Alvarado, J.L.; Bang, I.C.; Bishnoi, S.W.; Bonetti, M.; Botz, F.; Cecere, A.; Chang, Y.; Chen, G.; Chen, H.; Chung, S.J.; Chyu, M.K.; Das, S.K.; Paola, R.D.; Ding, Y.; Dubois, F.; Dzido, G.; Eapen, J.; Escher, W.; Funfschilling, D.; Galand, Q.; Gao, J.; Gharagozloo, P.E.; Goodson, K.E.; Gutierrez, J.G.; Hong, H.; Horton, M.; Hwang, S.K.; Iorio, C.S.; Jang, S.P.; Jarzelski, A.B.; Jiang, Y.; Jin, L.; Kabelac, S.; Kamath, A.; Kedzierski, M.A.; Kieng, L.G.; Kim, C.; Kim, J.H.; Kim, S.; Lee, S.H.; Leong, K.C.; Manna, I.; Michel, B.; Ni, R.; Patel, H.E.; Philip, J.; Poulikakos, D.; Reynaud, C.; Savino, R.; Singh, P.K.; Song, P.; Sundararajan, T.; Timofeeva, E.; Tricak, T.; Turanov, A.N.; Vaerenbergh, S.V.; Wen, D.; Witharana, S.; Yang, C.; Yeh, W.H.; Zhao, X.Z.; Zhou, S.Q.; *Journal of Applied Physics*, **2009**, *106*, 094312.
DOI: [10.1063/1.3245330](https://doi.org/10.1063/1.3245330)
52. Grumezescu, A.M.; Saviuc, C.; Chifiriuc, M.C.; Hristu, R.; Mihaiescu, D.E.; Balaure, P.; Stanciu, G.; Lazar, V.; *IEEE Transactions on Nanobioscience*, **2011**, *10*, 269.
DOI: [10.1109/TNB.2011.2178263](https://doi.org/10.1109/TNB.2011.2178263)
53. Li, X.; Zhu, D.; Wang, X.; *Journal of Colloid and Interface Science*, **2007**, *310*, 456.
DOI: [10.1016/j.jcis.2007.02.067](https://doi.org/10.1016/j.jcis.2007.02.067)
54. Mahendran, V.; Philip, J.; *Appl. Phys. Lett.*, **2012**, *100*, 073104.
DOI: [10.1063/1.3684969](https://doi.org/10.1063/1.3684969)
55. Chen, L.; Xie, H.; Li, Y.; Wei Yu, W.; *Colloids and Surfaces A: Physicochem. Eng. Aspects*, **2008**, *330*, 176.
DOI: [10.1016/j.colsurfa.2008.07.047](https://doi.org/10.1016/j.colsurfa.2008.07.047)
56. Fedele, L.; Colla, L.; Bobbo, S.; Barison, S.; Agresti, F.; *Nanoscale Research Letters*, **2011**, *6*, 300.
DOI: [10.1186/1556-276X-6-300](https://doi.org/10.1186/1556-276X-6-300)
57. Yu, W.; S.U.S. Choi, S.U.S.; *Journal of Nanoparticle Research*, **2003**, *5*, 167.
DOI: [10.1023/A:1024438603801](https://doi.org/10.1023/A:1024438603801)
58. Atul Tiwari, Ashutosh Tiwari (Eds), *Bioengineered Nanomaterials*, CRC Press, USA, **2013**.
59. Cabaleiro, D.; Pastoriza-Gallego, M.J.; Gracia-Fernández, C.; Piñeiro, M.M.; Lugo, L.; *Nanoscale Research Letters*, **2013**, *8*, 286.
DOI: [10.1186/1556-276X-8-286](https://doi.org/10.1186/1556-276X-8-286)
60. Polidori, G.; Fohanno, S.; Nguyen, C.T.; *International Journal of Thermal Sciences*, **2007**, *46*, 739.
DOI: [10.1016/j.ijthermalsci.2006.11.009](https://doi.org/10.1016/j.ijthermalsci.2006.11.009)
61. Soltani, S.; Etemad, S.Gh.; Thibault, J.; *International Communications in Heat and Mass Transfer*, **2010**, *37*, 29.
DOI: [10.1016/j.icheatmasstransfer.2009.08.005](https://doi.org/10.1016/j.icheatmasstransfer.2009.08.005)
62. Chena, H.; Witharana, S.; Jina, Y.; Kim, C.; Ding, Y.; *Particuology*, **2009**, *7*, 151.
DOI: [10.1016/j.partic.2009.01.005](https://doi.org/10.1016/j.partic.2009.01.005)
63. Mostafizur, R.M.; Aziz, A.R.A.; Saidur, R.; Bhuiyan, M.H.U.; Mahbulul, I.M.; *International Journal of Heat and Mass Transfer*, **2014**, *77*, 765.
DOI: [10.1016/j.ijheatmasstransfer.2014.05.055](https://doi.org/10.1016/j.ijheatmasstransfer.2014.05.055)
64. Ashutosh Tiwari, Anthony PF Turner (Eds), *Biosensors Nanotechnology*, John Wiley & Sons, USA, **2014**.
65. Sundar, L.S.; Singh, M.K.; Ramana, E.V.; Singh, B.; Gra'cio, J.; Sousa, A.C.M.; *Scientific Reports*, **4**, 4039.
DOI: [10.1038/srep04039](https://doi.org/10.1038/srep04039)
66. Beheshti, A.; Shanbedi, M.; Heris, S.Z.; *J Therm Anal Calorim*, **2014**, *118*, 1451.
DOI: [10.1007/s10973-014-4048-0](https://doi.org/10.1007/s10973-014-4048-0)
67. Srikant, R.R.; Prasad, M.M.S.; Amrita, M.; Sitaramaraju; A.V.; Krishna, P.V.; *Proceedings of the Institution of Mechanical Engineers, Part B: Journal of Engineering Manufacture*, **2014**, *228*, 3.
DOI: [10.1177/0954405413497939](https://doi.org/10.1177/0954405413497939)
68. Ganguly, S.; Chakraborty, S.; *Journal of Applied Physics*, **2009**, *106*, 124309.
DOI: [10.1063/1.3270423](https://doi.org/10.1063/1.3270423)
69. Vek'as, L.; Bica, D.; Avdeev, M.V.; *China Particuology*, **2007**, *5*, 43.
DOI: [10.1016/j.cpart.2007.01.015](https://doi.org/10.1016/j.cpart.2007.01.015)
70. Parametthanuwat, T.; Rittidech, S.; *Nanoscale and Microscale Thermophysical Engineering*, **2013**, *17*, 216.
DOI: [10.1080/15567265.2013.776652](https://doi.org/10.1080/15567265.2013.776652)
71. Gautam, A.; Kshirsagar, A.; Biswas, R.; Banerjee, S.; Khanna, P.K.; *RSC Adv.*, **2016**, *6*, 2746.
DOI: [10.1039/C5RA20861K](https://doi.org/10.1039/C5RA20861K)
72. Bhagat, U.K.; More, P.V.; Khanna, P.K.; *SAJ Nanosci Nanotech*, **2015**, *1*, 101.
73. (a) Yang, Y.; Tian, C.; *Photochemistry and Photobiology*, **2012**, *88*, 816-823.
DOI: [10.1111/j.1751-1097.2012.01157.x](https://doi.org/10.1111/j.1751-1097.2012.01157.x)
(b) Bachilo, S.M.; Strano, M.S.; Kittrell, C.; Hauge, R.J.; Smalley, R.E.; Weisman, R.B.; *Science*, **2002**, *298*, 2361.
DOI: [10.1126/science.1078727](https://doi.org/10.1126/science.1078727)
74. Bagheri, S.; Shameili, K.; Hamid, S.B.A.; *Journal of Chemistry*, **2013**, Article ID 848205.
DOI: [10.1155/2013/848205](https://doi.org/10.1155/2013/848205)
75. Capek, I.; Tiwari, A. (Eds), Wiley and Sons, USA, **2015**.
76. Prabhu, Y.T.; Rao, K.V.; Kumar, V.S.S.; Kumari, B.S.; *World Journal of Nano Science and Engineering*, **2014**, *4*, 21.
DOI: [10.4236/wjnse.2014.41004](https://doi.org/10.4236/wjnse.2014.41004)
77. Chen, C.; Liu, Q.; Gao, S.; Li, K.; Xu, H.; Zaizhu Lou, Z.; Huang, B.; Dai Y.; *RSC Adv.*, **2014**, *4*, 12098.
DOI: [10.1039/c4ra00179f](https://doi.org/10.1039/c4ra00179f)
78. Nur, H.; *Materials Science and Engineering B*, **2006**, *133*, 49.
DOI: [10.1016/j.mseb.2006.05.003](https://doi.org/10.1016/j.mseb.2006.05.003)
79. Mondal, D.; Tiwari, A. (Eds), John Wiley & Sons, USA, **2012**.
80. Ohsaka, T.; Izumi, F.; Fujiki, Y.; *Journal of Raman Spectroscopy*, **1978**, *7*, 321.

- DOI:** [10.1002/jrs.1250070606](https://doi.org/10.1002/jrs.1250070606)
81. Borodko, Y.; Habas, S.E.; Koebel, M.; Yang, P.; Frei, H.; Somorjai, G.A.; *J. Phys. Chem. B*, **2006**, *110*, 23052.
DOI: [10.1021/jp063338+](https://doi.org/10.1021/jp063338+)
82. Gelder, J.D.; Gussem, K.D.; Vandenabeele, P.; Moens, L.; *J. Raman Spectrosc.*, **2007**, *38*, 1133.
DOI: [10.1002/jrs.1734](https://doi.org/10.1002/jrs.1734)
83. Koenig, J.L.; Angood, A.C.; *Journal of Polymer Science: Part A-2*, **1970**, *8*, 1787.
DOI: [10.1002/pol.1970.160081013](https://doi.org/10.1002/pol.1970.160081013)
84. Schuler, T.; Tremel, W.; *Chem. Commun.*, **2011**, *47*, 5208.
DOI: [10.1039/c0cc05717g](https://doi.org/10.1039/c0cc05717g)
85. Tiwari, A.; Tiwari, A.(Eds), John Wiley & Sons, USA, **2012**.
86. (a) Alvarado, E.; Torres-Martinez, L.M.; Fuentes, A.F.; Quintana, P.; *Polyhedron*, **2000**, *19*, 2345.
DOI: [10.1016/S0277-5387\(00\)00570-2](https://doi.org/10.1016/S0277-5387(00)00570-2)
(b) Gruijthuijsen, K. van; Obiols-Rabasa, M.; Heinen, M.; Nagele, G.; Stradner, A.; *Langmuir*, **2013**, *29* (36), 11199-11207,
DOI: [10.1021/la402104q](https://doi.org/10.1021/la402104q)
(c) Napper, D.H.; Netschey, A; *Journal of Colloid and Interface Science*, **1971**, *37*, 528-535
DOI: [10.1016/0021-9797\(71\)90330-4](https://doi.org/10.1016/0021-9797(71)90330-4)
(d) Choi, G.N.; Krieger, I.M; *Journal of Colloid and Interface Science*, **1986**, *113*, 101-113
DOI: [10.1016/0021-9797\(86\)90210-9](https://doi.org/10.1016/0021-9797(86)90210-9)
87. Zuo, R.; Du, G.; Zhang, W.; Liu, L.; Liu, Y.; Mei, L.; Li, Z.; *Advances in Materials Science and Engineering*, **2014**, *2014*, Article ID 170148, 7.
DOI: [10.1155/2014/170148](https://doi.org/10.1155/2014/170148)
88. Elghniji, K.; Ksibi, M.; Elaloui, E.; *Journal of Industrial and Engineering Chemistry*, **2012**, *18*, 178.
DOI: [10.1016/j.jiec.2011.11.011](https://doi.org/10.1016/j.jiec.2011.11.011)
89. Uddin, M.J.; Cesano, F.; Scarano, D.; Bonino, F.; Agostini, G.; Spoto, G.; Bordiga, S.; Zecchina, A.; *Journal of Photochemistry and Photobiology A Chemistry* **2008**, *199* (1): 64-72
DOI: [10.1016/j.jphotochem.2008.05.004](https://doi.org/10.1016/j.jphotochem.2008.05.004)
90. Sharma, Y.; Tiwari, A.; Kobayashi, H.(Eds), John Wiley & Sons, USA, **2013**.
91. Ali, R.; Siew, O.B.; *JurnalTeknologi*, **2006**, *45*(F), 31.
DOI: [10.11113/jt.v45.339](https://doi.org/10.11113/jt.v45.339)
92. Zhou, J.K.; Lv, L.; Yu, J.; Li, H.L.; Guo, P.Z.; Sun, H.; Zhao, X.S.; *J. Phys. Chem. C*, **2008**, *112*, 5316.
DOI: [10.1021/jp709615x](https://doi.org/10.1021/jp709615x)



A Monthly Journal

Publish your article in this journal

Advanced Materials Letters
Special Issue on Nanomaterials

Advanced Materials Letters is an official international journal of International Association of Advanced Materials (IAAM, www.iaamonline.org) published monthly by VBRI Press AB from Sweden. The journal is intended to provide high-quality peer-review articles in the fascinating field of materials science and technology particularly in the area of structure, synthesis and processing, characterisation, advanced-state properties and applications of materials. All published articles are indexed in various databases and are available download for free. The manuscript management system is completely electronic and has fast and fair peer-review process. The journal includes review article, research article, notes, letter to editor and short communications.

Editor-in-Chief
Ashutosh Tiwari
ashutosh.tiwari@vabripress.com

Copyright © 2017 VBRI Press AB, Sweden

www.vbripress.com/ami

Supporting information

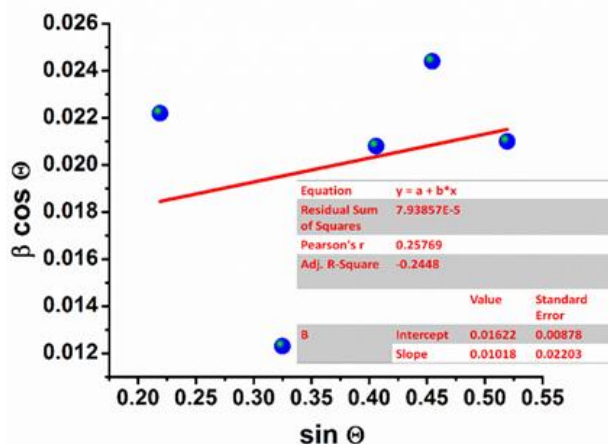


Fig. S1. Williamson-Hall plot of the titania nanoparticles.

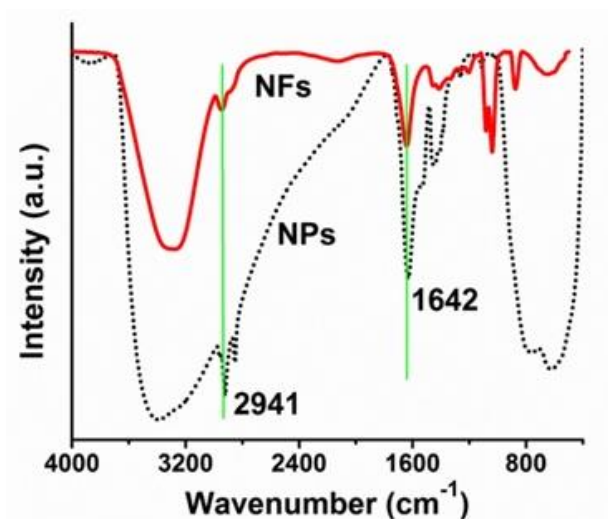


Fig. S2. FT-IR spectra of the anatase titania nanoparticles and NF.

Table S1. FTIR data of titania nanoparticles

Peak (cm ⁻¹)		Functional Group
Nano-Particles	Nano-Fluid	
-	521	Ti-O-Ti
-	596	Ti-O-Ti
623	651	Ti-O-Ti
775	-	Ti-O-Ti
-	870	Ti-O-Ti
-	1036	C-O
-	1083	C-O
1119	-	Ti-O-Ti
1263	1208	CH ₂ (rocking)
1448	-	CH ₂ (scissoring)
1642	1642	C=O
2851	2857	C-H (symm)
2941	2920	C-H (asymm)
3386	3283	-OH

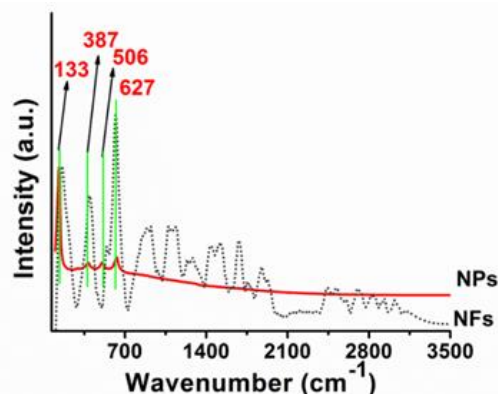


Fig. S3. Raman spectra of titania NPs and NF.

Table S2. Raman active modes in titania nanoparticles.

Peak (cm ⁻¹)		Raman active modes and Functional Groups
Nanoparticles	Nano-fluid	
132	160	Eg
187	-	Eg
387	404	B1g
505	518	B1g
627	618	Eg
PVP and EG		
-	754	C-C ring
-	851	C-C
-	933	C-C ring breathing
-	1023	C-C backbone
-	1344	
-	1370	CH deformation
-	1425	
-	1456	CH ₂ scissor
-	1494	
-	1675	C=O
OA		
-	1655	C=C vibration stretch
-	1265	=CH deformation
-	1301	CH ₂ deformation
-	800-850	CH ₂ stretching / rocking
-	1380	C-O-H bending
-	1100-1130	CH ₂ twisting
-	1420-1480	CH ₂ bending
-	2900	C-H antisymmetric

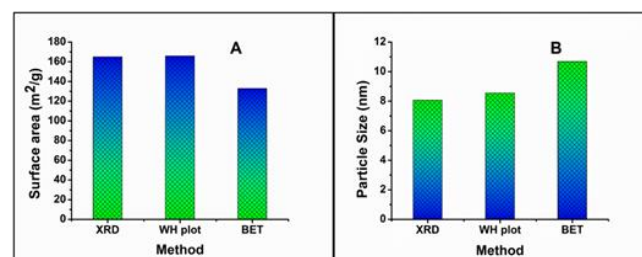


Fig. S4. Surface area and particle Size using XRD and BET analysis.

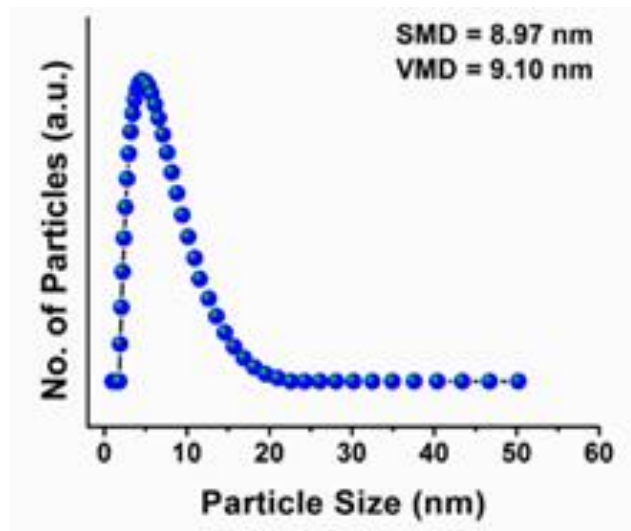


Fig. S5 Particle size distribution of the titania nanoparticles.

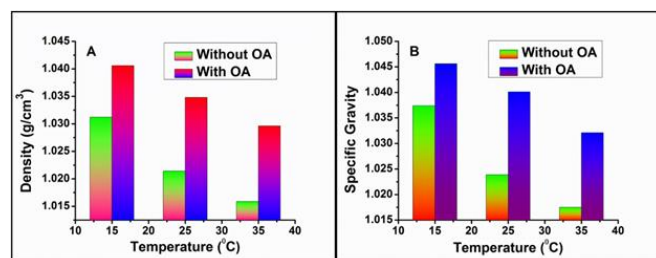


Fig. S6. (A) Density and (B) Specific gravity at varying temperature.

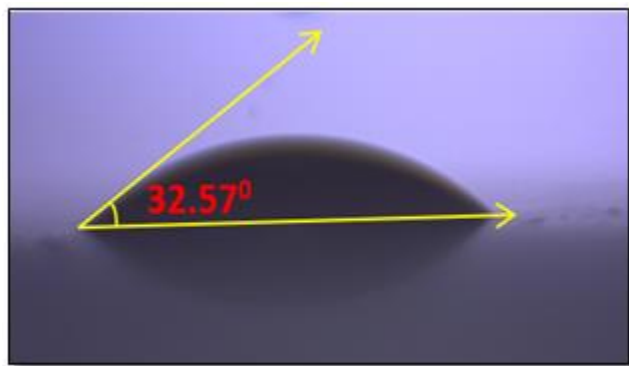


Fig. S7. Contact angle of the water droplet on drop casted nano-fluid on a glass slide.

Table S3. Some literature reports for MB dye degradation.

Reported by	Catalyst	% degradation	Time (min.)	Reference
Ksibiet <i>al</i>	TiO ₂	24	180	88
Zeechinaet <i>al</i>	Au doped TiO ₂	80	600	89
Wang <i>et al</i>	Cu doped TiO ₂	67	300	90
Ali <i>et al</i>	TiO ₂	26.37	300	91
Zhao <i>et al</i>	F doped TiO ₂	~80	480	92

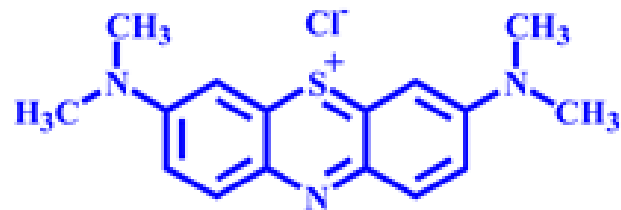


Fig. S8. Chemical Structure of Methylene Blue [71].

Table S4 Parameters for MB degradation under short UV irradiation.

Short UV Irradiation					
Concentration					
Dye (ppm)	Nano-fluid (mL)	Time (min)	Degradation Efficiency (%)	Rate (k) (min ⁻¹)	Ea (kJ mol ⁻¹)
05	01	270	61.43	0.0139	10652.12
	01	270	75.97	0.0157	10314.40
	1.5	270	78.84	0.0203	9721.59
15	02	270	84.60	0.0201	9735.81
	2.5	270	83.12	0.0290	9644.02
	03	270	88.11	0.0179	10026.99
	04	270	81.78	0.0194	9827.51
	05	270	86.87	0.0141	10622.81
25	01	270	47.84	0.0170	10164.55

Table S5 Parameters for dye degradation under long UV irradiation.

Long UV Irradiation					
Concentration					
Dye (ppm)	Nano-fluid (mL)	Time (min)	Degradation Efficiency (%)	Rate (k) (min ⁻¹)	Ea (kJ mol ⁻¹)
05	01	270	65.75	0.0172	10135.38
	1.5	270	55.12	0.0158	10347.17
	02	270	65.00	0.0152	10443.75
	2.5	270	68.29	0.0135	10739.63
	03	270	69.54	0.0154	10411.14
15	04	270	71.05	0.0135	10739.63
	05	270	68.61	0.0159	10331.43
	01	270	37.18	0.0190	9887.08
25	01	270	48.05	0.0193	9848.00